Mechatronics 37 (2016) 54–62

Contents lists available at ScienceDirect

Mechatronics

journal homepage: www.elsevier.com/locate/mechatronics

Shaping the trajectory of the billiard ball with approximations of the resultant contact forces

Grzegorz Kudra, Michał Szewc*, Igor Wojtunik, Jan Awrejcewicz

Lodz University of Technology, Department of Automation, Biomechanics and Mechatronics, Stefanowski St. 1/15, 90-924 Lodz, Poland

ARTICLE INFO

Article history:
Received 30 August 2015
Revised 23 November 2015
Accepted 3 January 2016
Available online 21 January 2016

Keywords:
Friction modelling
Coulomb–Contensou model
Parameter's optimization
Shaping the ball's trajectory

ABSTRACT

This paper presents mathematical models of the contact pressure distribution on a circular contact area and the corresponding rolling resistance. Hertzian pressure distribution is distorted in a special way in order to move rolling centre outside the geometrical centre of the contact area. With the assumption of fully developed sliding and classical Coulomb friction law on each element of the contact, integral models of the total friction force and moment reduced to the contact centre are given. In order to improve the convenience of use of the contact models in numerical simulations of rigid body dynamics and decrease their computational cost, special approximations of the integral models of friction force and moment are proposed. Moreover, special modifications of the corresponding expressions for friction forces and rolling resistance are proposed, which allows avoiding their singularities for vanishing relative motion of the contacting bodies. The application of the proposed contact models in mathematical modelling of a rigid ball rolling and sliding over a deformable table is presented. Furthermore, possibilities of use of the developed simulation models in shaping the billiard ball's trajectory are presented.

1. Introduction

Classical understanding of friction model is a relation between single component of friction force and one-dimensional relative displacement of the contacting bodies. This relation can possess different levels of complexity, beginning from the classical Coulomb law, ending on more advanced relations taking into account other properties of friction, including also additional state variables. These kinds of models are applied directly in mathematical descriptions and investigations of dynamical systems with frictional contacts, where at each point of the contact area the same relative motion of the contacting bodies takes place. Therefore, they can be also applied in the modelling of frictional contacts of bodies in three-dimensional space, if the contact can be considered as a point contact or plane and non-deformable without relative rotation of the contacting bodies in the contact plane.

However it occurs, that in the daily life one can encounter many examples of mechanical systems in three-dimensional space, where the assumption of the same relative motion of the contacting bodies at each point of the contact area is not fulfilled. One can enumerate here such examples like dynamics of rolling bearing, billiard ball, Thompson top, Celtic stone, wheel-soil or wheel-rail of the vehicles, and many others issues encountered in robotics. The local deformations of the bodies can be small enough with comparison to their dimensions, so the global motion of the bodies can be treated as rigid body motion. However, the shape and size of the contact zone can influence the global dynamics of the body. The full solution to this problem can be achieved with the use of space discretization and then one of such numerical methods like finite element method or, under special assumptions, the integration over the contact area. The last case corresponds to the assumptions used in the present paper. The space discretization leads however to significant increase of computational time. From the point of view of realistic and fast simulations of certain class of mechanical systems, it is important to construct special approximate models of the resultant contact forces.

Contensou in [1] indicated that moment of friction and relative angular velocity around the axis perpendicular to the contact plane can be very important in dynamics of some mechanical systems, i.e. quickly spinning tops. He presented analytical form (in terms of elliptic integrals) of dependence of the friction force on the relative sliding linear and angular velocities, assuming the classical Coulomb friction law and fully developed sliding on a circular contact area, with Hertzian contact pressure distribution. Zhuravlev in [2] showed that for a parabolic contact pressure distribution and a special choice of the co-ordinate system, one can find expressions for friction force and moment including only elementary functions.

* Corresponding author. Tel.: +48503142854.
E-mail addresses: grzegorz.kudra@p.lodz.pl (G. Kudra), michu.szewc@gmail.com (M. Szewc), igo90woj@interia.pl (I. Wojtunik), jan.awrejcewicz@p.lodz.pl (J. Awrejcewicz).

http://dx.doi.org/10.1016/j.mechatronics.2016.01.002
0957-4158/

Since these expressions are rather complicated and inconvenient in use for modelling of real systems and numerical simulations, he proposed special approximations of the exact expressions based on the Padé approximants as well. More results concerning the use of higher order Padé approximations in modelling friction force and moment are presented in [3]. Model of rolling resistance with the related special contact pressure distribution on circular contact area and the corresponding Padé approximations of the resultant friction force and moment were presented in [4]. Furthermore, the new families of models and approximations were proposed in [5], which can be understood as generalizations of the previously mentioned approaches. In particular, the model of contact pressure distribution and rolling resistance was extended to the case of elliptical contact area. Moreover, the approximations of the friction force and moment were generalized and their ability to fit the integral models or experimental data was increased.

The above mentioned integral models and their approximations concern the case of fully developed sliding. However, during simulations of mechanical systems one can manage not only with fully developed sliding, but also with stick mode, as well as transition between them. In general, there are three different approaches to this problem: time-stepping methods, event-driven methods and regularization methods. Kudra and Awrejcewicz in [6] presented numerical scheme and the corresponding examples of simulation of stick-slip oscillations, where both the linear and rotational relative motion of the contacting bodies takes place. The numerical algorithms were constructed as an event-driven scheme, where the approximations of the integral friction model for both the fully developed sliding and stick mode (determination of the end of the stick mode) were used. In [7] the corresponding regularized approximations of the integral models of friction for fully developed sliding were presented, where the singularities (for vanishing relative motion) were removed. It was shown that the developed models of friction lead to the same results as event-driven algorithm presented in [6].

The application of the special approximate model of the resultant contact forces in the billiard ball rolling and sliding on the deformable table is considered in this paper. Time consumption of the numerical calculation is crucial in simulation of the billiard game in which the models of resultant contact forces are expected to be computationally effective. Shaping the billiard ball's trajectory with the consideration of the influence of shape and size of the contact zone on the dynamics of the ball has not been found in the state of the art. Most of the found applications use the pre-prepared engines or large libraries without going into constituent parts. As it is written in [8], Open Dynamics Engine (ODE) is used. It is an open source physics library, which allows providing a realistic environment when 3D objects are colliding. ODE is used to simulate collisions between objects of different shapes. Another techniques and research to develop a game with reality is virtual reality technology with Visual, Auditory and Haptic Sensation presented in [9]. In [10] the simulation of the billiard game is based on the marker detection. However, none of them mentioned about the model of contact forces considering the shape and size of the contact zone and shaping the ball's trajectory. They focused on problem of collisions and communications between human and computer.

Section 2presents mathematical models of the contact pressure distribution, rolling resistance (2.1), integral model of friction force and moment (2.2) for fully developed sliding on a circular contact area, as well as their special approximations (2.3) and regularizations (2.4). Section 3 exhibits a mathematical model of a rigid billiard ball rolling and sliding over a deformable table (3.1). Additionally, this section presents the abilities of the developed models to predict and shape the billiard ball's trajectory. Section 4 contains some concluding remarks.

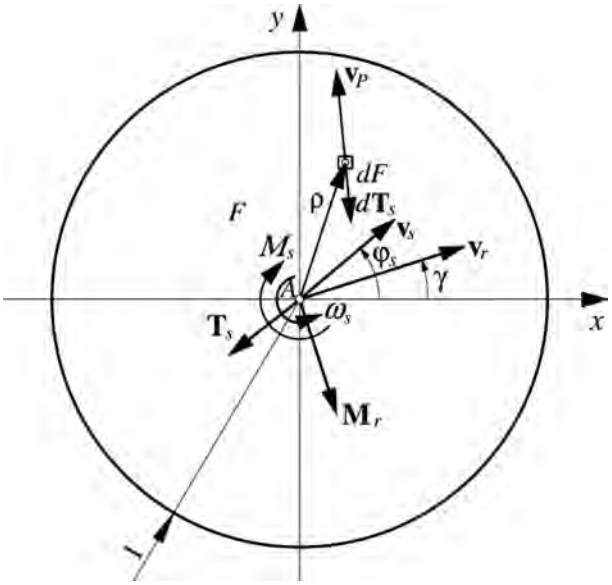

Fig. 1. The circular contact area with the characteristic relative velocities and the resultant forces and force couples acting on the body lying above the contact patch.

2. Modelling of the contact forces

2.1. Contact pressure distribution and rolling resistance

Let us consider a dimensionless circular contact area F presented in Fig. 1, with the Cartesian coordinate system $Axyz$ with axes xy lying in the contact plane. The dimensionless coordinates of a point situated on area F equals to $x = \hat{x}/\hat{a}$ and $y = \hat{y}/\hat{a}$, where $\hat{x}$ and $\hat{y}$ are the corresponding actual coordinates, while $\hat{a}$ is a radius of real contact.

The following form of non-dimensional contact pressure distribution [5] is assumed:

$$\sigma(x,y) = \hat{\sigma}(x,y)\frac{\hat{a}^2}{\hat{N}} = \frac{3}{2\pi}\sqrt{1-x^2-y^2}(1 + d_c x + d_s y) \tag{1}$$

where

$$d_c = d\cos\gamma = d\frac{v_{rx}}{\sqrt{v_{rx}^2 + v_{ry}^2}}$$
$$d_s = d\sin\gamma = d\frac{v_{ry}}{\sqrt{v_{rx}^2 + v_{ry}^2}} \tag{2}$$

In Eqs. (1–2) $\hat{\sigma}(x,y)$ denotes real contact pressure, $\hat{N}$,normal component of the real resultant force loading the contact, d, rolling resistance parameter, γ, angle describing "direction of rolling". The variables v_{rx} and v_{ry} are the components of the non-dimensional "rolling velocity" $\boldsymbol{v}_r = \hat{\boldsymbol{v}}_r/\hat{a} = v_{rx}\boldsymbol{e}_x + v_{ry}\boldsymbol{e}_y$ ($\hat{\boldsymbol{v}}_r$ is the corresponding real vector, $\boldsymbol{e}_\zeta$ is unit vector of axis $_\zeta$).

The model (1) is some artificial modification of the Hertzian stress distribution, moving the centre of the pressure distribution outside the geometrical centre A of the contact and allowing to model the non-dimensional rolling resistance. The latter finally reads

$$\boldsymbol{M}_r = \boldsymbol{f} \times \boldsymbol{e}_z = y_S\boldsymbol{e}_x - x_S\boldsymbol{e}_y = M_{rx}\boldsymbol{e}_x + M_{ry}\boldsymbol{e}_y \tag{3}$$

where

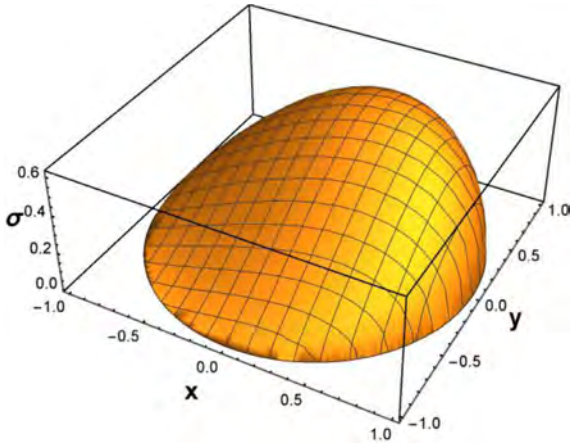

Fig. 2. The example of the contact pressure distribution (1–2), for $d = 1$ and $\gamma = 1$.

$$M_{rx} = \frac{1}{5}d_s \quad M_{ry} = -\frac{1}{5}d_c \tag{4}$$

and $\boldsymbol{f} = \overrightarrow{AS} = x_S\boldsymbol{e}_x + y_S\boldsymbol{e}_y$ is vector indicating position of the centre S of the non-dimensional contact pressure distribution. The centre S can be found using the following relations: $x_s = \iint_F \sigma(x,y)xdF$ and $y_s = \iint_F \sigma(x,y)ydF$. The real rolling resistance is $\hat{\boldsymbol{M}}_r = \hat{a}\hat{N}\boldsymbol{M}_r$.

Here some attention should be given to the introduced concept of "rolling direction" and "rolling velocity". In the case of contact of a deformable body and a rigid one, the "rolling direction" is a direction of relative motion of the centre of the contact area over the surface of the deformable body, while "rolling velocity" is the corresponding velocity. In the case of two deformable bodies, the rolling resistance can be modelled as a superposition of two independent rolling resistances, and the quantities d_c and d_s (2) can be understood as a resultant action of them. In the case of the system of billiard ball modelled in Section 3, it is assumed that a rigid ball rolls and slides over deformable table.

In Fig. 2 the example of the contact pressure distribution accordingly to the proposed model (1–2) is presented, where $d = 1$ and $\gamma = 1$ is assumed.

2.2. Integral model of the resultant friction forces

Assuming a fully developed sliding on the contact area F (see Fig. 1) and deformations of the bodies are small enough, we describe the relative motion of the two bodies in the contact plane as a plane motion of rigid bodies. This motion is characterized by the dimensionless linear sliding velocity in the centre A: $\boldsymbol{v}_s = \hat{\boldsymbol{v}}_s/\hat{a} = v_{sx}\boldsymbol{e}_x + v_{sy}\boldsymbol{e}_y$ and the angular sliding velocity: $\boldsymbol{\omega}_s = \hat{\boldsymbol{\omega}}_s = \omega_s\boldsymbol{e}_z$, where $\hat{\boldsymbol{v}}_s$ and $\hat{\boldsymbol{\omega}}_s$ are the corresponding real quantities.

Assuming sliding and applying the Coulomb friction law on each element dF of the contact, we get $d\boldsymbol{T}_s == d\hat{\boldsymbol{T}}_s/(\mu\hat{N}) = -\sigma(x,y)dF\,\boldsymbol{v}_P/\|\boldsymbol{v}_P\|$, where $d\boldsymbol{T}_s$ is elementary non-dimensional friction force, $d\hat{\boldsymbol{T}}_s$, its real counterpart, $\boldsymbol{v}_P$, local non-dimensional velocity of sliding and μ, dry friction coefficient. The moment of the friction force $d\boldsymbol{T}_s$ about the centre A of the contact reads $d\boldsymbol{M}_s = \boldsymbol{\rho}\times d\boldsymbol{T}_s = d\hat{\boldsymbol{M}}_s/(\hat{a}\mu\hat{N})$, where $d\hat{\boldsymbol{M}}_s$ is the corresponding real moment.

Summing up the elementary friction forces and moments, one get the following integral expressions for the corresponding components of the total friction force $\boldsymbol{T}_s = -T_{sx}\boldsymbol{e}_x - T_{sy}\boldsymbol{e}_y$ and moment $\boldsymbol{M}_s = -M_s\boldsymbol{e}_z$ reduced to point A:

$$T_{sx} = \iint_F \frac{\sigma(x,y)(v_{sx}-\omega_s y)}{\sqrt{(v_{sx}-\omega_s y)^2+(v_{sy}+\omega_s x)^2}}dxdy$$

$$T_{sy} = \iint_F \frac{\sigma(x,y)(v_{sy}+\omega_s x)}{\sqrt{(v_{sx}-\omega_s y)^2+(v_{sy}+\omega_s x)^2}}dxdy$$

$$M_s = \iint_F \sigma(x,y)\frac{\omega_s\left(x^2+y^2\right)+v_{sy}x-v_{sx}y}{\sqrt{(v_{sx}-\omega_s y)^2+(v_{sy}+\omega_s x)^2}}dxdy \tag{5}$$

where the signs have been changed in order to simplify further notation. The real quantities can then be calculated as $\hat{\boldsymbol{T}}_s = \mu\hat{N}\boldsymbol{T}_s$ and $\hat{\boldsymbol{M}}_s = \hat{a}\mu\hat{N}\boldsymbol{M}_s$.

The functions (5) possess redundancy in number of arguments. The used here kinematic quantities v_{sx}, v_{sy} and ω can be conveniently obtained during numerical simulations. They can be however reduced using the following relations

$$v_s = \lambda_s\cos\theta_s \quad \omega_s = \lambda_s\sin\theta_s \tag{6}$$

where

$$\lambda_s = \sqrt{v_s^2+\omega_s^2}$$

and

$$v_{sx} = v_s\cos\varphi_s \quad v_{sy} = v_s\sin\varphi_s \tag{7}$$

Taking into account the relation (6–7) in Eq. (5), one gets

$$T_{sx} = \iint_F \sigma(x,y)\frac{N_1}{D}dxdy \quad T_{sy} = \iint_F \sigma(x,y)\frac{N_2}{D}dxdy$$

$$M_s = \iint_F \sigma(x,y)\frac{N_3}{D}dxdy \tag{8}$$

where

$$N_1 = \cos\theta_s\cos\varphi_s - y\sin\theta_s$$

$$N_2 = \cos\theta_s\sin\varphi_s + x\sin\theta_s$$

$$N_3 = \left(x^2+y^2\right)\sin\theta_s + x\cos\theta_s\sin\varphi_s - y\cos\theta_s\cos\varphi_s$$

$$D = \sqrt{(\cos\theta_s\cos\varphi_s - y\sin\theta_s)^2+(\cos\theta_s\sin\varphi_s + x\sin\theta_s)^2}$$

The integral components (8) for the proposed contact pressure distribution (1– 2) possess the following properties

$$\begin{aligned}
&f(\theta_s,\varphi_s,\gamma) = -f(\theta_s+\pi,\varphi_s,\gamma) \text{ for } f = T_{sx}, T_{sy}, M_s\\
&f(\theta_s,\varphi_s,\gamma) = -f(-\theta_s,\varphi_s+\pi,\gamma) \text{ for } f = T_{sx}, T_{sy}, M_s\\
&f(\theta_s,\varphi_s,\gamma) = f(-\theta_s,\varphi_s,\gamma+\pi) \text{ for } f = T_{sx}, T_{sy}\\
&f(\theta_s,\varphi_s,\gamma) = -f(-\theta_s,\varphi_s,\gamma+\pi) \text{ for } f = M_s
\end{aligned} \tag{9}$$

The examples of the components T_{sx}, T_{sy} and M_s of the integral model (9) are presented in Fig. 3, where $\varphi_s = 0$ and $d = 1$ is assumed.

2.3. Approximations of the integral model of friction forces

Since the expressions (5) or (8) contain the integrals over the contact area, their direct use in numerical simulations may be inconvenient and time consuming. The exact analytical expressions exist, but they are also inconvenient because of their complexity [1– 4]. In this situation one can use the following approximations of the corresponding components of the integral model:

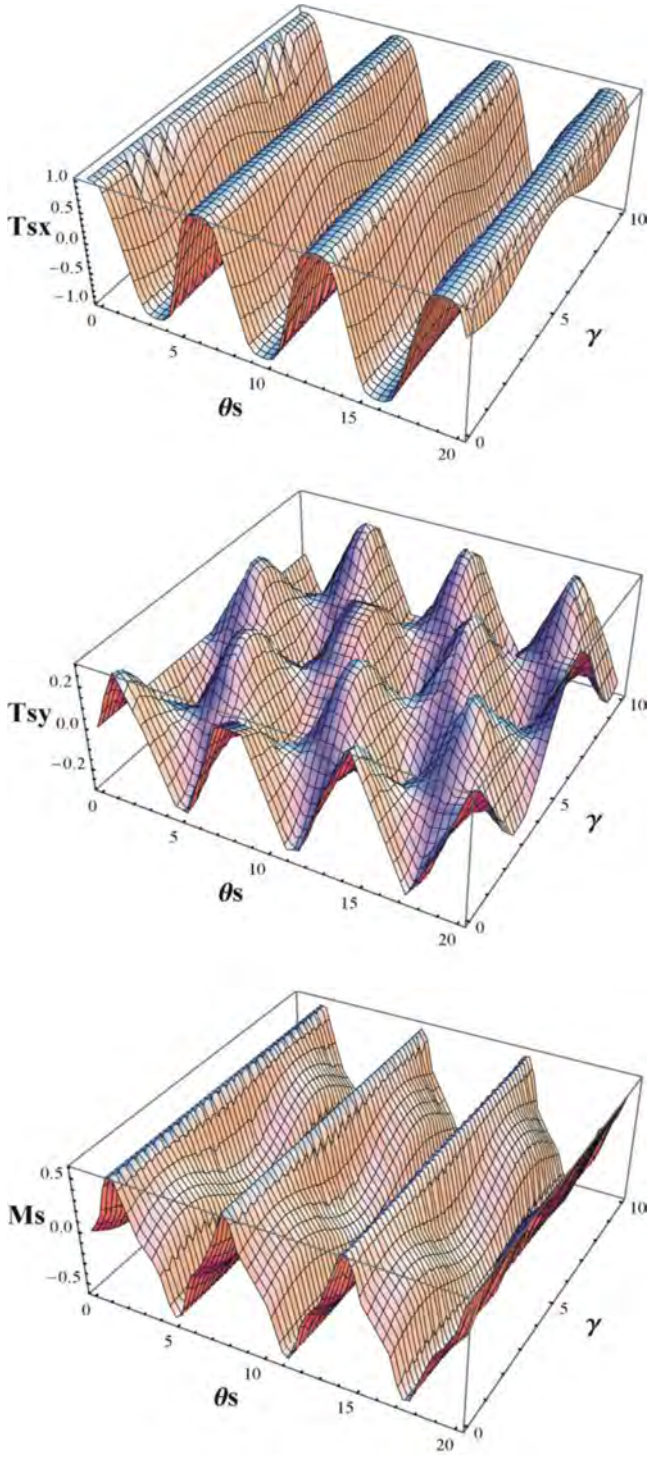

Fig. 3. The components (T_{sx}, T_{sy}, M_s) of the integral friction model (9), for $d = 1$, $\varphi_s = 0$.

$$T_{sx}^{(I)} = \frac{v_{sx} - b_T c_{0,1,1}^{(x,y)} \omega_s}{\left(|v_s|^{m_T} + b_T^{m_T} |\omega_s|^{m_T}\right)^{m_T^{-1}}}$$

$$T_{sy}^{(I)} = \frac{v_{sy} + b_T c_{1,0,1}^{(x,y)} \omega_s}{\left(|v_s|^{m_T} + b_T^{m_T} |\omega_s|^{m_T}\right)^{m_T^{-1}}}$$

$$M_s^{(I)} = \frac{b_M c_{0,0,-1}^{(x,y)} \omega_s - c_{0,1,0}^{(x,y)} v_{sx} + c_{1,0,0}^{(x,y)} v_{sy}}{\left(b_M^{m_M} |\omega_s|^{m_M} + |v_s|^{m_M}\right)^{m_M^{-1}}} \tag{10}$$

where

$$c_{i,j,k}^{(x,y)} = \iint_F x^i y^j \left(x^2 + y^2\right)^{-\frac{k}{2}} \sigma(x,y)\, dxdy$$

which belongs to the larger family of approximations proposed in the work [5] and fulfilling conditions (9).

The components (9) fulfil the following conditions

$$f^{(I)}\big|_{v_s=0} = f|_{v_s=0}$$
$$f^{(I)}\big|_{\omega_s=0} = f|_{\omega_s=0} \tag{11}$$

where $f = T_{sx}, T_{sy}, M_s$ are the corresponding integral components. The constant parameters b_T, m_T, b_M and m_M do not influence the conditions (11) and can be found in the process of optimization by fitting the approximate components to the exact integral ones. They can be identified from the experimental data as well.

For the model of the contact pressure distribution (1) one get

$$c_{0,1,1}^{(x,y)} = \frac{3}{32}\pi d_s \quad c_{1,0,1}^{(x,y)} = \frac{3}{32}\pi d_c$$
$$c_{0,0,-1}^{(x,y)} = \frac{3}{16}\pi \quad c_{0,1,0}^{(x,y)} = \frac{1}{5} d_s \quad c_{1,0,0}^{(x,y)} = \frac{1}{5} d_c \tag{12}$$

Using the relation (6–7) and changing the kinematic variables, the expressions (9) take the following form:

$$T_{sx}^{(I)} = \frac{\cos\theta_s \cos\varphi_s - b_T c_{0,1,1}^{(x,y)} \sin\theta_s}{\left(|\cos\theta_s|^{m_T} + b_T^{m_T} |\sin\theta_s|^{m_T}\right)^{m_T^{-1}}}$$

$$T_{sy}^{(I)} = \frac{\cos\theta_s \sin\varphi_s + b_T c_{1,0,1}^{(x,y)} \sin\theta_s}{\left(|\cos\theta_s|^{m_T} + b_T^{m_T} |\sin\theta_s|^{m_T}\right)^{m_T^{-1}}}$$

$$M_s^{(I)} = \frac{b_M c_{0,0,-1}^{(x,y)} \sin\theta_s - c_{0,1,0}^{(x,y)} \cos\theta_s \cos\varphi_s + c_{1,0,0}^{(x,y)} \cos\theta_s \sin\varphi_s}{\left(b_M^{m_M} |\sin\theta_s|^{m_M} + |\cos\theta_s|^{m_M}\right)^{m_M^{-1}}} \tag{13}$$

Taking into account the properties (9) and the circularity of the contact, it is sufficient to compare the integral and approximate models only on the region $D \equiv \{(d,\ \gamma,\ \theta_s)$: $0 \le d \le 1,\ 0 \le \gamma \le \pi,\ -\pi/2 \le \theta_s \le \pi/2\}$, assuming $\varphi_s = 0$. Therefore, in the process of the approximate model's optimization, the following objective functions are constructed

$$F_T(b_T, m_T) = \int_D \left(\left(T_{sx} - T_{sx}^{(I)}\right)^2 + \left(T_{sy} - T_{sy}^{(I)}\right)^2\right) dD$$
$$F_M(b_M, m_M) = \int_D \left(M_s - M_s^{(I)}\right)^2 dD$$

allowing to find the following set of optimal parameters: $b_T = 0.771$, $m_T = 2.655$, $b_M = 0.419$ and $m_M = 3.073$. The optimization process has also been carried out assuming that $m_T = 2$ and $m_M = 2$, which resulted in the following parameters: $b_T = 0.68102$, $b_M = 0.480909$. This assumption leads to the significant reduction of the computational time in some cases.

Fig. 4 exhibits comparison of the full integral model (8) of friction forces (T_{sx}, T_{sy}, M_s) for $\varphi_s = 0$, $d = 0.6$ and $\gamma = 1$, with the optimized approximate models (13) in the two above mentioned cases: where all the parameters are optimized ($T_{sx}^{(Ia)}$, $T_{sy}^{(Ia)}$, $M_s^{(Ia)}$) and where $m_T = 2$ and $m_M = 2$ ($T_{sx}^{(Ib)}$, $T_{sy}^{(Ib)}$, $M_s^{(Ib)}$) is assumed.

2.4. Regularizations of the models of friction and rolling resistance

The models of rolling resistance and friction forces presented in the previous sections, concern the case of non-zero rolling velocity and fully developed sliding. They possess singularities for vanishing rolling resistance or lack of relative sliding motion. The full models of rolling resistance and friction should be the set-valued

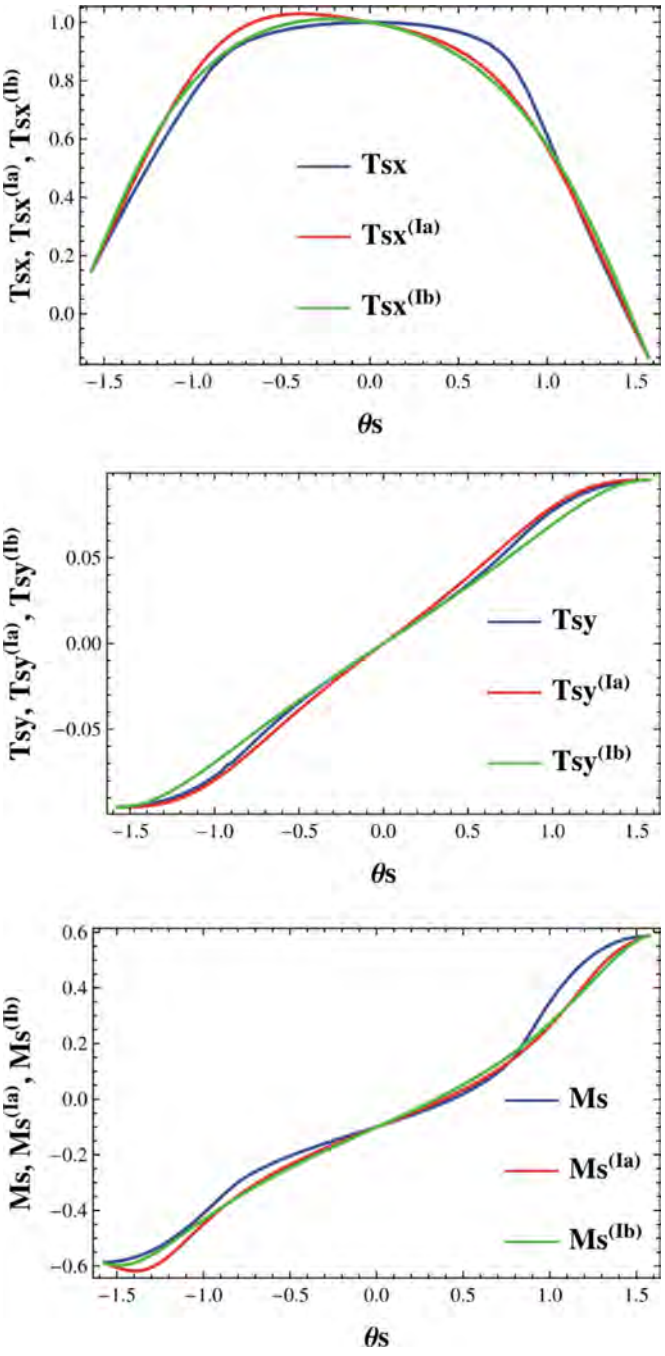

Fig. 4. Comparison of the optimized approximations (13) with the full integral model of friction (8).

models taking into account both stick and motion (rolling and sliding) modes, as well the transition between them. One can however simplify the problem making the special changes in the corresponding expressions for rolling resistance (deformation of the contact pressure) and friction components during sliding, obtaining their smooth (regularized) counterparts.

In the case of regularization of the rolling resistance, one should introduce in the denominators of the expressions (2) a small numerical parameter ε_r, obtaining the following smooth versions of these expressions

$$d_{c\varepsilon} = d\frac{v_{rx}}{\sqrt{v_{rx}^2 + v_{ry}^2 + \varepsilon_r^2}} \quad d_{s\varepsilon} = d\frac{v_{ry}}{\sqrt{v_{rx}^2 + v_{ry}^2 + \varepsilon_r^2}} \tag{14}$$

Then the rolling resistance reads

$$\boldsymbol{M}_{r\varepsilon} = M_{rx\varepsilon}\boldsymbol{e}_x + M_{ry\varepsilon}\boldsymbol{e}_y \tag{15}$$

where

$$M_{rx\varepsilon} = \frac{1}{5}d_{s\varepsilon} \quad M_{ry\varepsilon} = -\frac{1}{5}d_{c\varepsilon}$$

The real regularized rolling resistance is then equal to $\hat{\boldsymbol{M}}_{r\varepsilon} = \hat{a}\hat{N}\boldsymbol{M}_{r\varepsilon}$.

In order to eliminate the singularities from the integral expression for components of friction model, we introduce the small parameter ε_t in the following way

$$\begin{aligned}
T_{sx\varepsilon} &= \iint_F \frac{\sigma(x,y)(v_{sx} - \omega_s y)}{\sqrt{(v_{sx} - \omega_s y)^2 + (v_{sy} + \omega_s x)^2 + \varepsilon_t^2}}dxdy \\
T_{sy\varepsilon} &= \iint_F \frac{\sigma(x,y)(v_{sy} + \omega_s x)}{\sqrt{(v_{sx} - \omega_s y)^2 + (v_{sy} + \omega_s x)^2 + \varepsilon_t^2}}dxdy \\
M_{s\varepsilon} &= \iint_F \sigma(x,y)\frac{\omega_s\left(x^2 + y^2\right) + v_{sy}x - v_{sx}y}{\sqrt{(v_{sx} - \omega_s y)^2 + (v_{sy} + \omega_s x)^2 + \varepsilon_t^2}}dxdy
\end{aligned} \tag{16}$$

The total regularized friction force and moment read $\boldsymbol{T}_{s\varepsilon} = -T_{sx\varepsilon}\boldsymbol{e}_x - T_{sy\varepsilon}\boldsymbol{e}_y$ and $\boldsymbol{M}_{s\varepsilon} = -M_{s\varepsilon}\boldsymbol{e}_z$, correspondingly. Their real counterparts are $\hat{\boldsymbol{T}}_{s\varepsilon} = \mu\hat{N}\boldsymbol{T}_{s\varepsilon}$ and $\hat{\boldsymbol{M}}_{s\varepsilon} = \hat{a}\mu\hat{N}\boldsymbol{M}_{s\varepsilon}$.

The approximate models of friction force and moment are regularized in an analogical way, adding a small parameter ε_t in the denominators of the corresponding expressions:

$$\begin{aligned}
T_{sx\varepsilon}^{(I)} &= \frac{v_{sx} - \frac{3}{32}\pi b_T d_{s\varepsilon}\omega_s}{\sqrt{\left(|v_s|^{m_T} + b_T^{m_T}|\omega_s|^{m_T}\right)^{2m_T^{-1}} + \varepsilon_t^2}} \\
T_{sy\varepsilon}^{(I)} &= \frac{v_{sy} + \frac{3}{32}\pi b_T d_{c\varepsilon}\omega_s}{\sqrt{\left(|v_s|^{m_T} + b_T^{m_T}|\omega_s|^{m_T}\right)^{2m_T^{-1}} + \varepsilon_t^2}} \\
M_{s\varepsilon}^{(I)} &= \frac{\frac{3}{16}\pi b_M\omega_s - \frac{1}{5}d_{s\varepsilon}v_{sx} + \frac{1}{5}d_{c\varepsilon}v_{sy}}{\sqrt{\left(b_M^{m_M}|\omega_s|^{m_M} + |v_s|^{m_M}\right)^{2m_M^{-1}} + \varepsilon_t^2}}
\end{aligned} \tag{17}$$

The corresponding non-dimensional friction force and moment are then computed as $\boldsymbol{T}_{s\varepsilon}^{(I)} = -T_{sx\varepsilon}^{(I)}\boldsymbol{e}_x - T_{sy\varepsilon}^{(I)}\boldsymbol{e}_y$ and $\boldsymbol{M}_{s\varepsilon}^{(I)} = -M_{s\varepsilon}^{(I)}\boldsymbol{e}_z$, while their real counterparts read $\hat{\boldsymbol{T}}_{s\varepsilon}^{(I)} = \mu\hat{N}\boldsymbol{T}_{s\varepsilon}^{(I)}$ and $\hat{\boldsymbol{M}}_{s\varepsilon}^{(I)} = \hat{a}\mu\hat{N}\boldsymbol{M}_{s\varepsilon}^{(I)}$, respectively.

3. Billiard ball

3.1. Mathematical model

An example of application of the presented model is a billiard ball rolling and sliding on deformable table, presented in Fig. 5, where the following notation is used: $\boldsymbol{v}$, velocity of the ball centre O; $\hat{\boldsymbol{T}}_{s\varepsilon}$, the resultant friction force acting at the contact centre A; $\hat{\boldsymbol{N}} = \hat{N}\boldsymbol{e}_z$, the normal reaction acting on the ball; $\hat{\boldsymbol{\omega}}_s$, angular sliding velocity; $\hat{\boldsymbol{v}}_{\boldsymbol{r}}$, linear rolling velocity; $\hat{\boldsymbol{M}}_{s\varepsilon}$, moment of friction forces; $\hat{\boldsymbol{M}}_{r\varepsilon}$, moment of rolling resistance; $\hat{\boldsymbol{v}}_{\boldsymbol{s}}$, linear sliding velocity at the point A. It is assumed that a rigid ball rolls and slides over the deformable table, therefore $\hat{\boldsymbol{v}}_{\boldsymbol{r}} = \boldsymbol{v}$.

Since the permanent contact between the ball and table is assumed with constant normal reaction $\hat{N} = mg$, the billiard ball is governed by the following set of differential equations:

$$m\frac{d\boldsymbol{v}}{dt} = \hat{\boldsymbol{T}}_{s\varepsilon} \tag{18a}$$

$$\boldsymbol{B}\frac{d\boldsymbol{\omega}}{dt} = \boldsymbol{r} \times \hat{\boldsymbol{T}}_{s\varepsilon} + \hat{\boldsymbol{M}}_{s\varepsilon} + \hat{\boldsymbol{M}}_{r\varepsilon} \tag{18b}$$

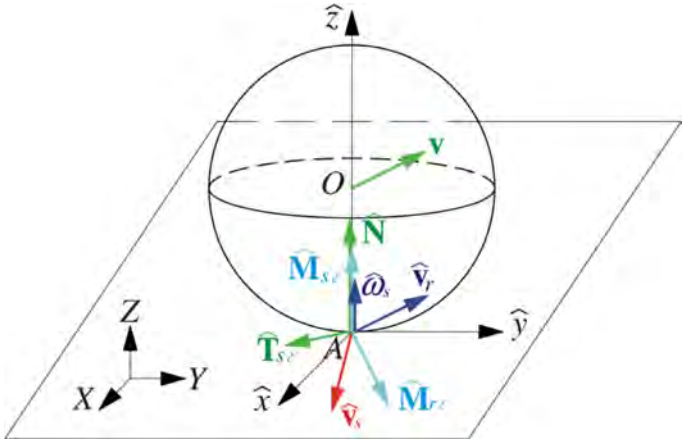

Fig. 5. The contact area of the billiard ball.

where $\boldsymbol{r} = \overrightarrow{OA}$, m denotes mass of the ball, while $\mathbf{B}$ is tensor of inertia in the mass centre O.

Using the matrix representation one can write:

$$\boldsymbol{v} = \begin{bmatrix} v_x \\ v_y \\ v_z \end{bmatrix} \quad \boldsymbol{\omega} = \begin{bmatrix} \omega_x \\ \omega_y \\ \omega_z \end{bmatrix} \quad \boldsymbol{r} = \begin{bmatrix} 0 \\ 0 \\ -r \end{bmatrix}$$

$$\hat{\boldsymbol{T}}_{s\varepsilon} = \begin{bmatrix} \hat{T}_{sx\varepsilon} \\ \hat{T}_{sy\varepsilon} \\ 0 \end{bmatrix} = \mu mg \begin{bmatrix} T_{sx\varepsilon} \\ T_{sy\varepsilon} \\ 0 \end{bmatrix} \quad \hat{\boldsymbol{M}}_{s\varepsilon} = \begin{bmatrix} 0 \\ 0 \\ \hat{M}_{s\varepsilon} \end{bmatrix} = \hat{a}\mu mg \begin{bmatrix} 0 \\ 0 \\ M_{s\varepsilon} \end{bmatrix}$$

$$\hat{\boldsymbol{M}}_{r\varepsilon} = \begin{bmatrix} \hat{M}_{rx\varepsilon} \\ \hat{M}_{rx\varepsilon} \\ 0 \end{bmatrix} = \hat{a}mg \begin{bmatrix} M_{rx\varepsilon} \\ M_{rx\varepsilon} \\ 0 \end{bmatrix} \quad \boldsymbol{B} = \begin{bmatrix} B & 0 & 0 \\ 0 & B & 0 \\ 0 & 0 & B \end{bmatrix} \tag{19}$$

where $B = 2/5mr^2$ is the central inertia moment of the body.

Vector product can be expressed in different forms (vector or matrix):

$$\boldsymbol{r} \times \hat{\boldsymbol{T}}_{s\varepsilon} = \begin{vmatrix} \boldsymbol{e}_x & \boldsymbol{e}_y & \boldsymbol{e}_z \\ 0 & 0 & -r \\ \hat{T}_{sx\varepsilon} & \hat{T}_{sy\varepsilon} & 0 \end{vmatrix} = r\hat{T}_{sy\varepsilon}\boldsymbol{e}_x - r\hat{T}_{sx\varepsilon}\boldsymbol{e}_y$$

or

$$\boldsymbol{r} \times \hat{\boldsymbol{T}}_{s\varepsilon} = \begin{bmatrix} 0 & r & 0 \\ -r & 0 & 0 \\ 0 & 0 & 0 \end{bmatrix} \cdot \begin{bmatrix} \hat{T}_{sx\varepsilon} \\ \hat{T}_{sy\varepsilon} \\ 0 \end{bmatrix} = \begin{bmatrix} r\hat{T}_{sy\varepsilon} \\ -r\hat{T}_{sx\varepsilon} \\ 0 \end{bmatrix} = \mu mg \begin{bmatrix} rT_{sy\varepsilon} \\ -rT_{sx\varepsilon} \\ 0 \end{bmatrix} \tag{20}$$

Eq. (18a) leads to the following two scalar differential equations governing the mass centre of the ball:

$$\frac{dv_x}{dt} = -\mu g T_{sx\varepsilon}, \quad \frac{dv_y}{dt} = -\mu g T_{sy\varepsilon} \tag{21}$$

while the third equation is $dv_z/dt = 0$. Assumption of permanent contact results in five degrees of freedom of the analysed system.

Applying relation (19–20) to Eq. (18b) one could obtain the following differential equations governing the angular motion of the ball

$$\begin{aligned} \frac{d\omega_x}{dt} &= -\frac{5}{2}\frac{g}{r}\left(\mu T_{sy\varepsilon} - \frac{1}{r}\hat{a}M_{rx\varepsilon}\right) \\ \frac{d\omega_y}{dt} &= \frac{5}{2}\frac{g}{r}\left(\mu T_{sx\varepsilon} + \frac{1}{r}\hat{a}M_{ry\varepsilon}\right) \\ \frac{d\omega_z}{dt} &= -\frac{5}{2}\frac{g}{r^2}\hat{a}\mu M_{s\varepsilon} \end{aligned} \tag{22}$$

For computation of the absolute position of the ball centre one need the following additional equations:

$$\frac{dX_O}{dt} = v_x, \quad \frac{dY_O}{dt} = v_y \tag{23}$$

where X_O and Y_O are the coordinates of the ball centre O in the global coordinate system XYZ.

In order to apply the proposed models of friction forces one also need

$$\hat{\boldsymbol{v}}_s = \boldsymbol{v}_A = \boldsymbol{v} + \boldsymbol{\omega} \times \boldsymbol{r} \tag{24}$$

Representing Eq. (24) in the matrix form one get

$$\begin{bmatrix} v_{sx} \\ v_{sy} \\ v_{sz} \end{bmatrix} = \begin{bmatrix} v_{Ax} \\ v_{Ay} \\ v_{Az} \end{bmatrix} = \begin{bmatrix} v_x \\ v_y \\ v_z \end{bmatrix} + \begin{bmatrix} 0 & -\omega_z & \omega_y \\ \omega_z & 0 & -\omega_x \\ -\omega_y & \omega_x & 0 \end{bmatrix} \cdot \begin{bmatrix} 0 \\ 0 \\ -r \end{bmatrix} \tag{25}$$

which finally takes the following form:

$$v_{sx} = \frac{v_x - r\omega_y}{\hat{a}} \quad v_{sy} = \frac{v_y + r\omega_x}{\hat{a}} \quad v_{sz} = 0 \tag{26}$$

In the rolling resistance model one use the following relation

$$v_{rx} = \frac{v_x}{\hat{a}} \quad v_{ry} = \frac{v_y}{\hat{a}} \tag{27}$$

3.2. Possibilities of shaping the ball's trajectory

Results of simulation of the ball's motion in the two cases are presented: (i) the instance where the full integral models of friction forces ($T_{sx\varepsilon}$, $T_{sy\varepsilon}$, $M_{s\varepsilon}$) are applied; (ii) the instance where the integral models are replaced by the corresponding approximants ($T^{(I)}_{sx\varepsilon}$, $T^{(I)}_{sy\varepsilon}$, $M^{(I)}_{s\varepsilon}$). Proper set of the initial conditions may result in obtaining the desired trajectory.

The comparison of the full integral model with the approximate model is presented in Figs. 6–8. However, because of the difficulty of carrying out calculations with some initial conditions, only the results of approximate model are presented in Figs. 9–10.

In Fig. 6 the straight motion of the ball along the direction of Y axis is presented. The diagonal movement of the ball is presented in Fig 7. Fig. 8 shows the reversal motion of the ball along the Y direction. Fig. 9 shows the case, in which ball is turning in direction X and then it is doing a curve motion in the opposite direction. Fig. 10 exhibits the case in which the ball is turning in both X and Y direction at the same time, and then it constantly rolls in both X and Y direction until it stops.

For the approximate model the following parameters were used: $\hat{a} = 0.003\,\mathrm{m}$, $\mu = 0.2$, $d = 1$, $\varepsilon_t = 0.01$, $\varepsilon_r = 0.01$, $g = 9.81\,\mathrm{m/s^2}$, $r = 0.02\mathrm{m}$, $m_T = 2$, $m_M = 2$, $b_T = 0.68102$, $b_M = 0.480909$. Some of the initial conditions are the same for each of the presented simulations: $X_O(0) = 0$, $Y_O(0) = 0$, $\alpha_x(0) = 0$, $\alpha_y(0) = 0$, $\alpha_z(0) = 0$, $v_x(0) = 0$ and $v_y(0) = 1$. The rest of them are different for the particular figures and they are noted in the figures' descriptions.

During the simulations the approximate models of friction forces with the parameters $m_T = m_M = 2$ were used, since they occur computationally more effective than the corresponding models with the different values of the m_T and m_M.

4. Concluding remarks

In the work simplified models of the friction force and moment are presented, as well as rolling resistance for fully developed sliding on a circular contact area with Coulomb friction law valid on each of its element. Then the introduced contact models are applied in modelling and numerical simulations of a rigid billiard ball rolling and sliding over a deformable table. The proposed approximated models of friction forces occurred very effective and able

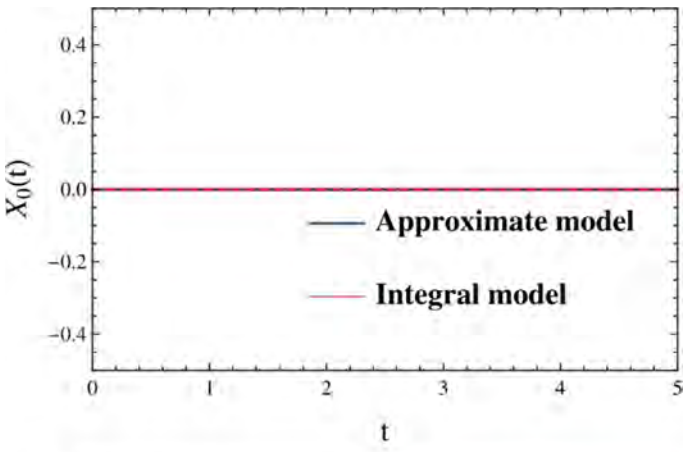

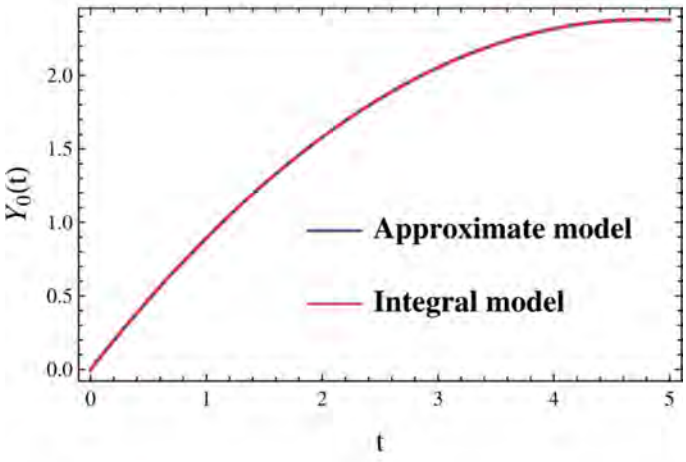

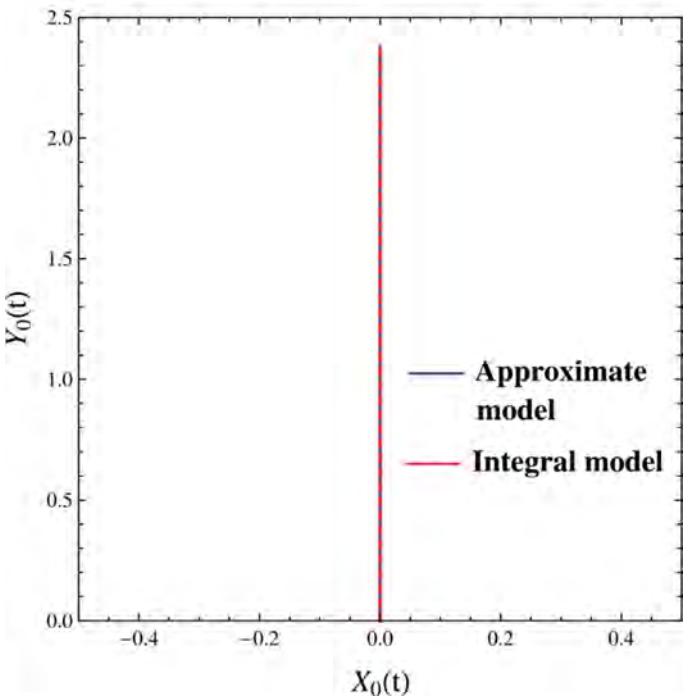

Fig. 6. Position of the billiard ball during the straight motion. Initial conditions: $\omega_x(0) = -50$ rad/s, $\omega_y(0) = 0$ and $\omega_z(0) = 0$.

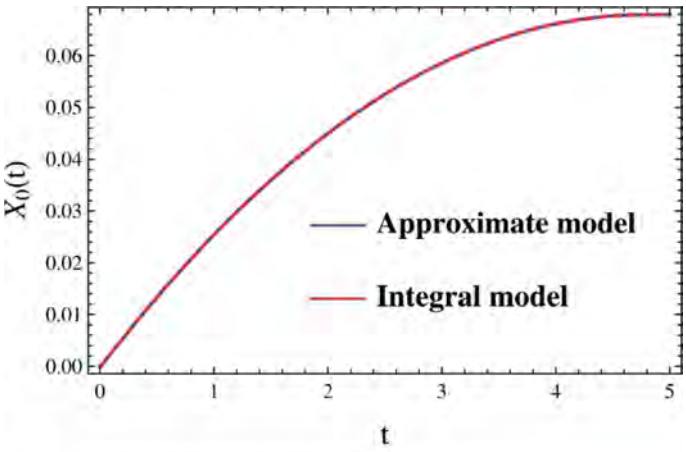

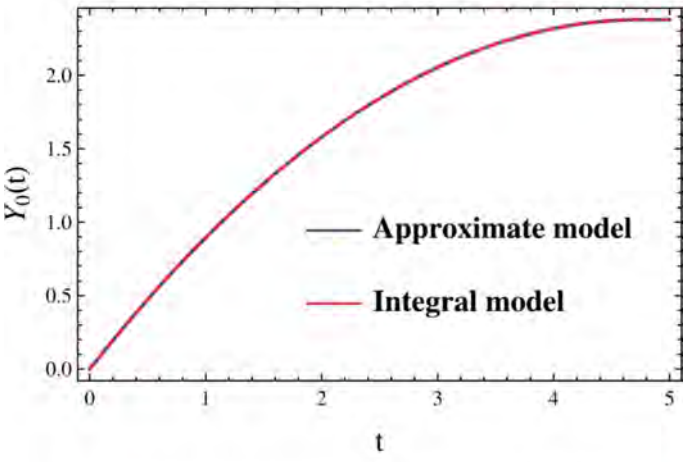

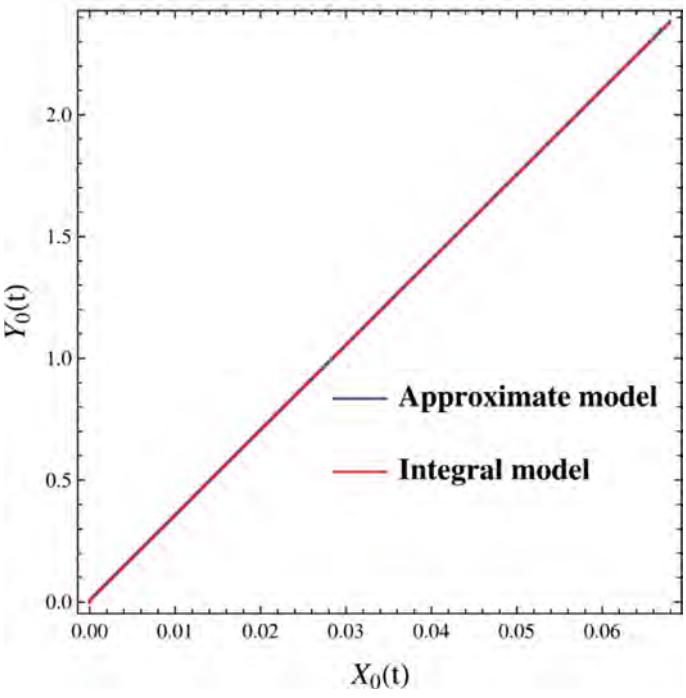

Fig. 7. Position of the billiard ball during the diagonal movement. Initial conditions: $\omega_x(0) = -50$ rad/s, $\omega_y(0) = 5$ rad/s and $\omega_z(0) = 0$.

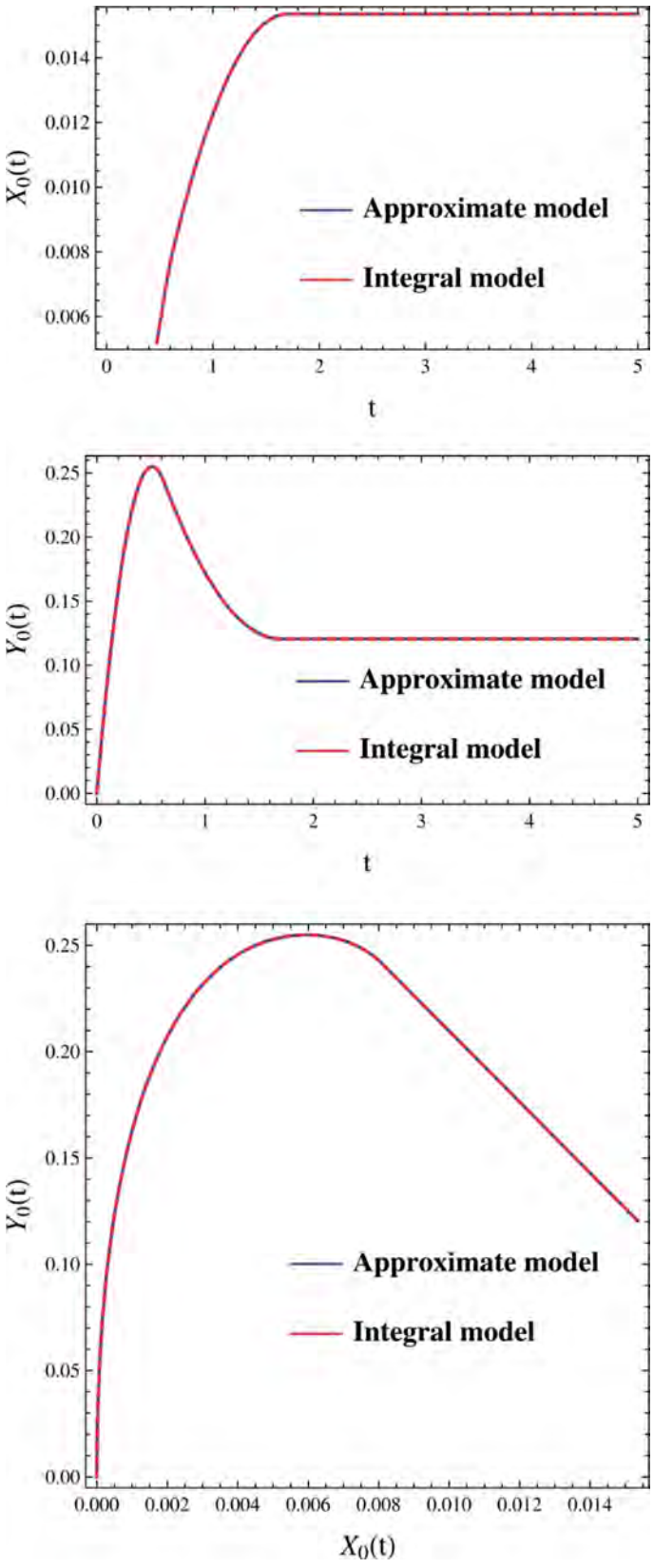

Fig. 8. Position of the billiard ball during turning in x direction. Initial conditions: $\omega_x(0) = 150$ rad/s, $\omega_y(0) = 5$ rad/s and $\omega_z(0) = 0$.

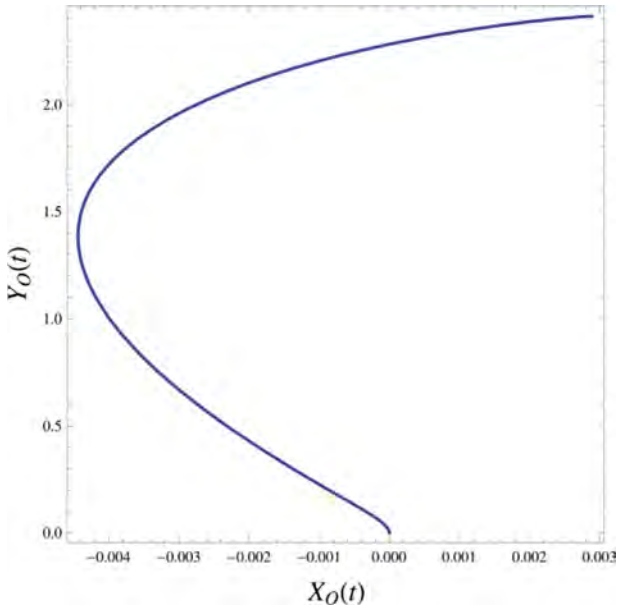

Fig. 9. Position of the billiard ball during the curve movement. Initial conditions: $\omega_x(0) = -50$ rad/s, $\omega_y(0) = -3.5$ rad/s and $\omega_z(0) = -150$ rad/s.

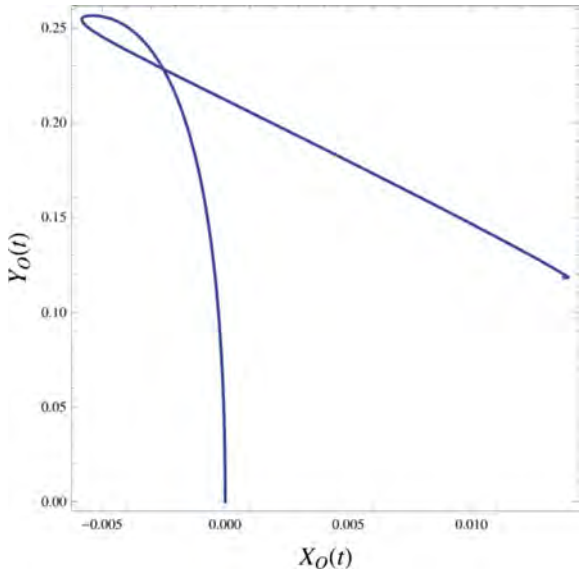

Fig. 10. Position of the billiard ball during full turn movement. Initial conditions: $\omega_x(0) = 150$ rad/s, $\omega_y(0) = 0$ and $\omega_z(0) = -150$ rad/s.

to substitute inconvenient and extremely computationally expensive integral expressions. They can be used in fast numerical simulations of rigid body dynamics, computer games or control algorithms based on the plant model.

The presented results of simulations of the billiard ball indicate large possibilities of shaping the ball's trajectory by manipulating its initial conditions. Thus, the developed models can be potentially used as elements of control system of a machine playing billiard. They should be supplemented by models of impacts between the ball and other objects like another billiard ball, cue or table band.

The parameters of the developed contact models have been found in the process of optimization of fitting the approximate models to the corresponding integral expressions. Note however, that these and other parameters of the contact models can be also estimated based on the experimental data. To collect such data, a special control and test station should be constructed. Therefore,

the use of different mechatronic sensors such as high speed camera, 3D scanner, laser scanner is being analysed by the paper's authors. Placing inertial measurement unit (IMU) with the wireless data transmission inside the moving ball is considered as well. With such test station and the results presented in this study, proposed friction force and moment model could be verified.

Acknowledgment

This work was supported by the Polish National Science Centre, MAESTRO 2, No. 2012/04/A/ST8/00738.

References

[1] Contensou P. Couplage entre frottement de glis sement et de pivotement dans la téorie de la toupe. In: Ziegler H, editor. Kreiselprobleme Gyrodynamic. Berlin: Springer-Verlag Ed; 1962. IUTAM Symposium Celerina p. 201–16.
[2] Zhuravlev VP. The model of dry friction in the problem of the rolling of rigid bodies. J Appl Math Mech. 1998;62(5):705–10.
[3] Zhuravlev VP, Kireenkov AA. Padé expansions in the two-dimensional model of Coulomb friction. Mech Solids 2005;40(2):1–10.
[4] Kireenkov AA. Combined model of sliding and rolling friction in dynamics of bodies on a rough plane. Mech Solids 2008;43(3):412–25.
[5] Kudra G, Awrejcewicz J. Approximate modelling of resulting dry friction forces and rolling resistance for elliptic contact shape. Eur J Mech Solids 2013;42:358–75.
[6] Kudra G, Awrejcewicz J. Bifurcational dynamics of a two-dimensional stick-slip system. Differ Eq Dyn Syst 2012;20(3):301–22.
[7] Kudra G, Awrejcewicz J. Regularized model of coupled friction force and torque for circularly-symmetric contact pressure distribution. In: Proceedings of the 11th Conference on Dynamical Systems - Theory and Applications; 2011. p. 353–8.
[8] Yersin B, Ciger J. The virtual billiard game. Virtual Reality Lab. Lausanne, Switzerland: Swiss Federal Institute of Technology; 2004. p. 3–9.
[9] Takamura Y, Abe N, Tanaka K, Taki H, He S. A virtual billiard game with visual, auditory and haptic sensation. Technologies for E-Learning and Digital Entertainment. Lect Notes Comput Sci 2006;3942:700–5.
[10] De Paolis LT, Aloisio G, Pulimeno M. A simulation of a billiards game based on marker detection. In: Second International Conferences on Advances in Computer-Human Interactions Cacun Mexico; 2009. p. 148–51.